THERMAL FATIGUE APPEARS TO BE MORE DAMAGING THAN UNIAXIAL ISOTHERMAL FATIGUE FOR THE AUSTENTIC STAINLESS STEELS, AND APPLICATION OF MULTIAXIAL FATIGUE CRITERIA

Antoine Fissolo *
CEA – Saclay
DM2S/SEMT/LISN Bat 607
91191 Gif sur Yvette, France
Phone: 33 1 69 08 31 02, Fax: 33 1 69 08 87 84
antoine.fissolo@cea.fr

Sébastien Amiable **Andrei Constantinescu**
École Polytechnique
Laboratoire de Mécanique des Solides - CNRS UMR 7649,
91128 Palaiseau, France

Olivier Ancelet **Stéphane Chapuliot** **Cédric Gourdin**
CEA – Saclay
DM2S/SEMT/LISN, Bat 607 91191 Gif sur Yvette, France

Adrien Demassieux
INSA Rouen
Avenue de l'Université, BP 8 76801 St Etienne du Rouvray, France

Ludovic Vincent
CEA – Saclay
DMN/SRMA /LCD Bat 455 91191 Gif sur Yvette, France

Jean Marc Stelmaszyk
Institut de Radioprotection et de Sûreté Nucléaire
BP17 92262 Fontenay-aux-Roses, France

ABSTRACT: For nuclear reactor components, uniaxial isothermal fatigue curves are used to estimate the crack initiation under thermal fatigue. However, such approach would be not sufficient in some cases where cracking was observed. To investigate differences between uniaxial and thermal fatigue damage, tests have been carried out at CEA using the thermal fatigue devices SPLASH and FAT3D: a bi-dimmensionnal (2-D) loading status is obtained in SPLASH, whereas a tri-dimensional (3-D) loading status is obtained in FAT3D. All the analysed tests clearly show that crack initiation in thermal fatigue is faster than in uniaxial isothermal fatigue conditions: for identical levels of strain, the number of cycles required to achieve crack initiation is significantly lower. The enhanced damaging effect probably results from a pure mechanical origin: a nearly perfect biaxial state corresponds to an increased hydrostatic stress. Consequently, multiaxial fatigue criteria must be applied. The Zamrik's strain criterion and the energy criterion proposed by Ecole Polytechnique provide the best estimations. Furthermore, application of the Zamrik's criterion using the RCC-MR method seems to be promising.

Key words: PWR, thermal fatigue, biaxial stress, fatigue initiation, crack initiation

1. Introduction

Thermal fatigue induces in-service damage in various industrial components, such as moulds, rolling mill cylinders or turbine blades. Some examples are given by [1], [2], [3]. It also occurs in different types of nuclear reactor components. In Liquid Metal Fast Breeder Reactors (LMFBRs), strong thermal fatigue fluctuations may be generated by incomplete mixing of sodium flows at different temperatures, or by a cyclical movement of sodium stratification interface. In the case of Pressurized Water Reactors (PWRs), networks of cracks may appear in auxiliary cooling lines, close to cold-water injection sites, in spite of the relatively small temperature fluctuations [4], [5]. In May 1998, a leak occurred in the reactor heat removal system (RHRS) of the Civaux 1 plant. The major cause of cracking was identified as high cycle thermal fatigue [6], [7]. In the following years, a multi-discipline strategy has been adopted by CEA to investigate thermal fatigue [8].

In France, estimations of fatigue resistance of nuclear reactor components are based both on the RCC-M design code (close to the ASME code) and on the French RCC-MR code. The first was specifically developed for PWRs design. The second was developed for the Fast Breeder Reactor design. Such methodologies assume that thermal fatigue resistance on components can be directly extrapolated from classical push-pull tests (performed with stress or strain range controls). However, cracking damage in some instances (RHRS…), resulting from thermal fatigue loading, would indicate the necessity to investigate such hypotheses more precisely.

The present study focuses on crack initiation under thermal fatigue. In this framework, we will use data obtained from specific tests [9], [10], [11]. Experimental tests were carried out for initiating crack damage and for developing networks of cracks under thermal fatigue loading. Thermal fatigue campaigns have been conducted at CEA using SPLASH and FAT3D facilities. In the first test, 2-D rectangular section specimens were used [12]. On the second test, although the specimen is a simple tube, 3-D loadings were applied because local gradients are combined with global gradients [13], [14], [15]. An important push-pull test campaign was also conducted to investigate a potential discrepancy between thermal and isothermal fatigue. More tests were performed for both conditions and specimens from the same heat, so as to prevent chemical composition or fabrication variability from affecting the interpretation of the results.

2. Thermal fatigue tests

Thermal fatigue results are obtained using SPLASH and FAT3D facilities located at CEA. As for in-service components, thermo-mechanical loadings directly result from temperature gradients along the wall thickness. However, the main difference between the two facilities is the following: the first test uses 2-D specimens whereas the second test uses 3-D tubular specimens, with a non axis-symmetrical loading. The facilities, experimental procedures and experimental results are detailed hereafter.

SPLASH tests: Temperature gradients are produced in 2-D specimens using the SPLASH equipment. Fig. 1 presents the SPLASH testing facility and the SPLASH specimen.

The test facility is composed of a massive, rigid specimen (240x30x20 mm^3) continuously heated by an electrical DC current and cyclically cooled by water sprayed on the two opposites faces of the specimen, as displayed in Fig. 1. Thermal down-shocks produced by cyclic water spraying induce large temporal and spatial gradients: the cooling-rate is about 600 °C/s and the gradient along the specimen depth is approximately 100 °C/mm. The thermal loading zone is confined to a few square millimetres on the surface and a few millimetres in depth. These loading conditions yield a small-localized plastic zone, where the crack network evolves. The temporal surface temperature range and temperature gradient during quenching are nearly equal (a temporal temperature range of 150°C in surface roughly corresponds to a 160 °C gradient in the thickness direction).

Two types of specimens are used: calibration specimens and endurance specimens. Both are equipped with K-type thermocouples brazed in depth, at 3 and 7-mm from the left and right surfaces. To obtain complete temperature maps on the surface and to verify thermocouple measurements, additional temperature measurements are now performed on the surface of the quenched zone using an infra-red camera [16].

Steels studied here are AISI 304 L and AISI 316 L(N) type austenitic stainless steels, with an average grain size of about 50-µm. The chemical composition of the steels is specified in Table 1.

Table 1.
Chemical compositions (wt %) of 304 L and 316 L(N) stainless steels.

	C	Mn	Si	Cr	Ni	Mo	S	P	N	Fe
304 L	0.031	1.48	0.55	19.4	8.6	0.23	0.003	0.028	0.058	Bal.
316 L(N)	0.024	1.82	0.46	17.44	12.33	2.3	0.001	0.003	0.06	Bal.

After crack initiation, crack growth, coalescence and finally networks of cracks can be observed. At the end of the test, the 3-D character of the networks of cracks can be examined, morphological parameters can be determined, using a step-by-step removal of thin layers. For more information, one can refer to [12], [17]. The present study only deals with crack initiation.

Figure 2 gives the evolution of the temperature range as a function of the number of cycles to crack initiation. As the temperature range increases, a very sharp decrease of the number of cycles to initiation N_i is observed. When temporal ΔT on surface ranges from 100 to 125 °C, no cracks are detected, even after 10^6 cycles, whereas with a ΔT of 300 °C, initiation occurs after only 6,000 cycles when T_{max} = 550°C. As for isothermal fatigue, a fatigue limit can be clearly defined: it simply corresponds to the temperature range for which no cracking is observed.No significant difference between the two tested materials is observed in the low cycle thermal fatigue regime.

Only the last testing campaign, performed at the maximum temperature of 320 °C with 304L steel specimens is analysed. This choice was made to ensure that all the thermal fatigue tests have been performed under strictly identical conditions (same water spray pistols, same electrical conditions …). Furthermore, a comparison between thermal fatigue and isothermal push-pull tests will be performed on specimens of the same heat of 304 L steel, in order to avoid a potential variability effect. The analysed tests thus correspond to only a small fraction of the SPLASH campaigns (Fig. 2-b).

FAT3D tests: Fig. 3 presents the FAT3D facility and principle. The main goal of this test is to evidence the role of 3-D loadings on damage. In addition, the loading configurations are simple enough to be reproduced by numerical simulations. The specimen is a simple tube. To obtain a homogeneous heating, it is placed in an oven. Cold water is periodically injected on the inner skin, at a single and fixed position. More precisely, injected water boundaries roughly had a parabolic shape. This effectively generates 3-D loadings, because local gradients (T differences between inner and outer skins) are combined with global gradients (T differences between the sides of the tube). Obviously, as for SPLASH tests, the thermal cycle in FAT3D test includes a cooling part and a heating part.

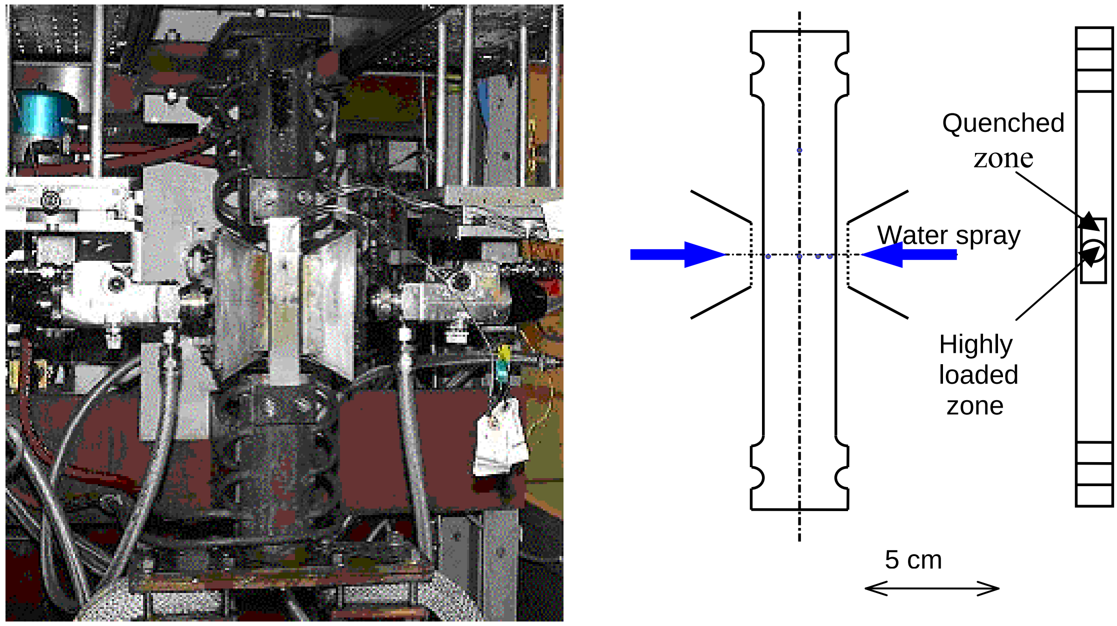

Fig. 1: SPLASH facility and specimen

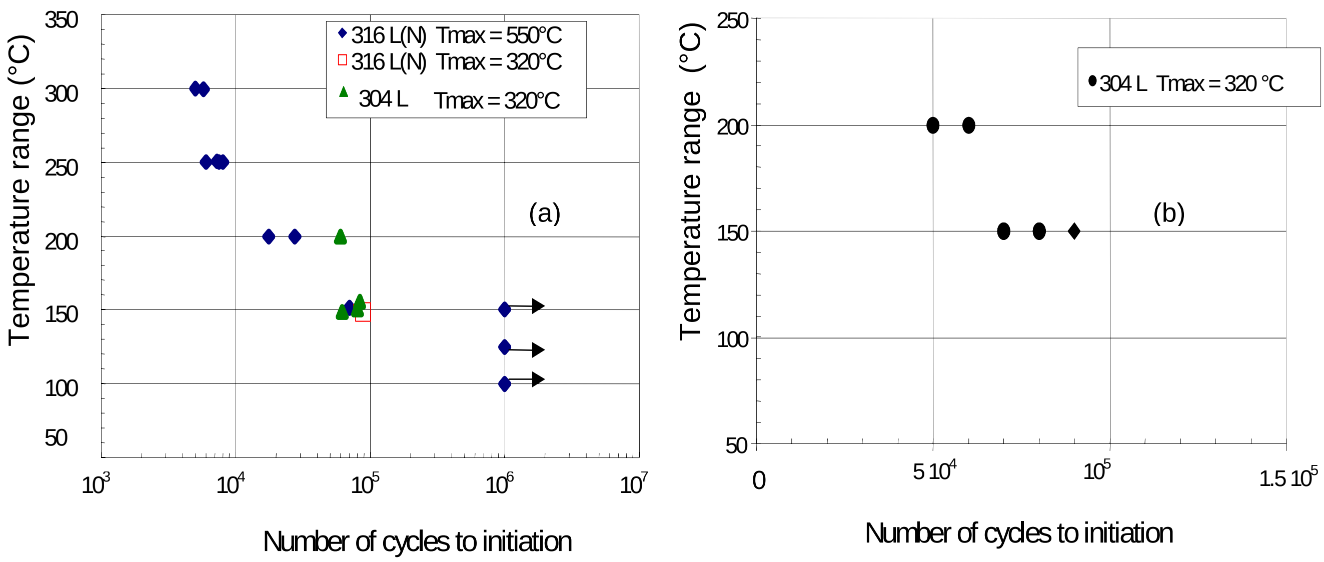

Fig. 2: 20 years testing SPLASH data base, number of cycles to initiation versus the temperature range on surface during quenching. (a), tests performed only on 304L steel (b).

Temperatures are monitored using K thermocouples. As for the SPLASH test, a calibration specimen is used to determine thermal loading. That specimen is equipped with 19 thermocouples placed in the outer skin and across the wall thickness, at the position of the cooling zone (0.7 and 3.5-mm from the internal skin). In order to place thermocouples through the thickness, a specific hole is machined and plugged with metal. For each fatigue experiment, the FAT3D tube is also equipped with 19 thermocouples, placed on the outer skin only.

Specimens are 316L 360-mm tall steel tubes, with a 170-mm outer diameter and a 6.7-mm wall thickness (Fig. 3). The cooling zone is detailed on Fig. 3-b. The top part corresponds to the highest load zone, in contrast with the SPLASH 2-D specimen, where the highest load zone is the centre of the quenched zone. The FAT3D loading configuration comes from a 3-D structure effect. This analysis was plainly confirmed by the emergence of damage. Initiation was defined as a “mechanically significant crack”. Such definition corresponds to 1 to 2 millimetres long crack on the surface. Three tests have been performed on 316 L steel specimens. Chemical composition is given in Table 2:

Table 2
Chemical composition of 316 L steel used for FAT3D tests (in Weight %).

C	Mn	Si	Cr	Ni	Mo	S	P	Co	Fe
0.051	2.14	0.39	16.13	8.10	2.23	0.010	0.015	0.013	Balance

For each test, data presented in Table 3 show:

1 - A number of cycles for which no any crack is detected.
2 - A number of cycles for which one (or several) crack(s) is detected, that occurrence corresponding to the first crack observation.
3 - The higher coordinate-Z where the last crack is observed when the test ends. These cracks are ca. 2 millimetres long on the surface.

In order to investigate the impact of multiaxiality, such results have been compared with uniaxial low cycle fatigue data (strain control conditions) obtained on the same 316L heat. LCF tests have been performed at room temperature, instead of at the temperature representative of the thermal cycling (for example at the average temperature of the cycle in a SPLASH test). However, RCC-MR data shows only a slight temperature effect for endurance: LCF at 450 °C [18], [19] corresponds roughly to LCF at 20 °C by changing N_R by $N_R/2$ (Fig. 4).

Indeed, to compare endurance on TF with endurance on LCF, the estimation of a “reference temperature” for LCF is not easy. However, the minimum temperature seems to be a more relevant choice: the water quenched zone is mainly loaded under tension during the cooling stage and mainly under compression during the heating stage. Table 3 shows that minimum and average temperatures in the outer wall are lower than 450°C (Outer minimum temperature = Outer maximum temperature – ΔT), and closer instead to 200 °C and 300 °C respectively. In addition, the inner-wall temperatures are obviously even lower. As a result, the comparison with LCF at 450°C and N_R, or with LCF at room temperature and $N_R/2$ are representative and somewhat conservative.

Furthermore, as suggested by the RCC-MR data, the effect of temperature on hardening is negligible in the 20–450 °C temperature range. Therefore, the mechanical constitutive behaviour is simply fitted to room temperature LCF data.

The next part deals with thermal and mechanical analysis of both SPLASH and FAT3D results.

Table 3
FAT3D main experimental conditions and results.

	FAT3D -1		FAT3D -2		FAT3D -3	
Total cycle duration $t_c + t_f$ (seconds)	190		130		91	
Cooling duration t_f (seconds)	15		15		11	
Outer maximum temperature (°C)	530		470		440	
Outer skin ΔT (°C)	360		290		220	
1 - Number of cycles for which no any crack are detected	3800		21417		14186	
2 - Number of cycles with crack and surface length (mm)	11845	30	30093	15	22923	6
Total number of cycles	17532		30093		48147	
3 - The higher height-Z where the last crack is observed when test is ended (mm) left-side / right-side	195	185	207	210	158	169

3. Thermal and mechanical analysis

The thermo-mechanical state of specimens is determined from two uncoupled computations: first a thermal analysis, then a mechanical analysis using the previously computed temperature field as input parameters. The uncoupling hypothesis is based on the negligible thermal heating due to the inelastic deformation, compared to the global heating problem.

The constitutive behaviour is uncoupled from the damage evolution. This assumption has already been validated in a series of papers [20], [21].

Another hypothesis assumes that stabilized stress-strain behaviour is obtained after a short transition period. Let us note that the RCC-MR method [18] also make the same assumption, since a K_v coefficient allows the calculation of an elasto-plastic strain from a pure elastic calculation. As previously observed on 316 L(N) steel [22], the evolution of stress in a cyclic experiment is quite complex. It can be typically described using a series of superposed hardening laws as proposed in [23]. Therefore, we shall make some simplifying assumptions, supposing that the behaviour of the material is stabilized after a first hardening period and that all computations will take place in this area. Such an assumption appears to be sufficient in our case.

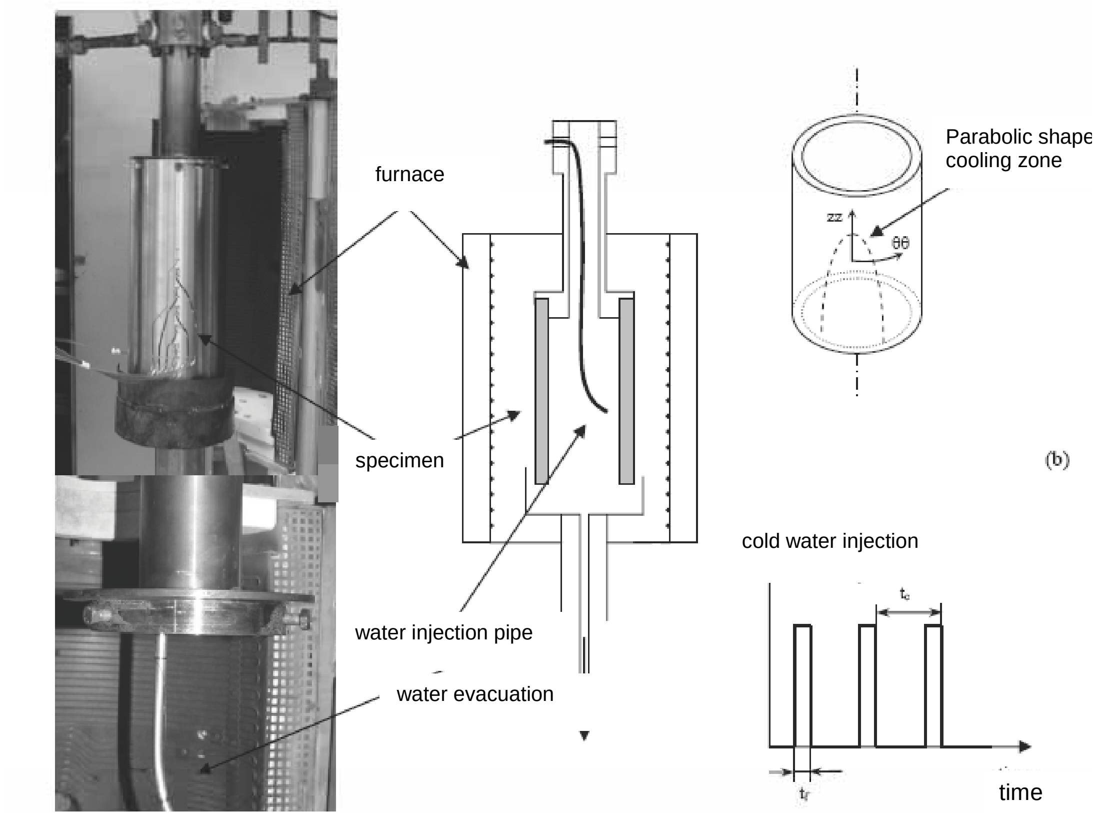

Fig. 3: FAT3D facility and principle.

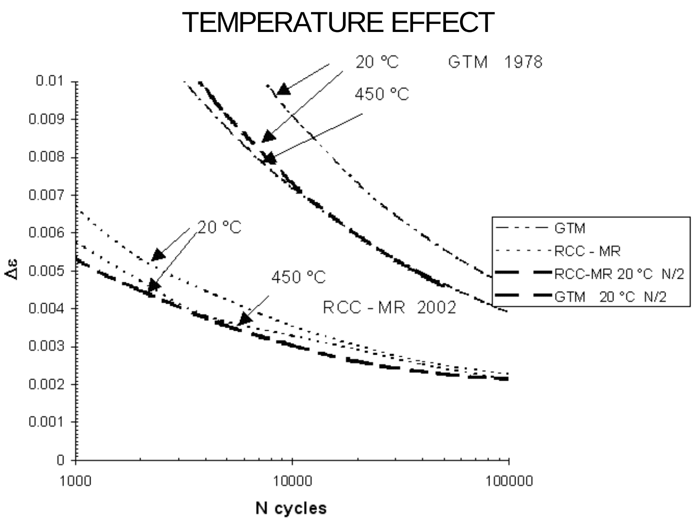

Fig. 4: 316 L steels - Experimental curves and Design RCC-MR curves. Comparison between 450 °C – N_R curves, 20 °C – N_R curves and 20 °C – $N_R/2$ curves.

More precisely, two types of 3-D mechanical calculations have been conducted for both facilities: the first is a pure elastic calculation to be applied using the French code RCC-MR estimation, which is based on the modified Poisson coefficient [24], [25], the second is an elasto-plastic calculation based on stabilised cyclic elasto-plastic behaviour law (non-linear kinematic law).

The elasto-plastic constitutive behaviour is fitted on low cycle fatigue test results at $N_R/2$ (equations 2). They are given by:

$\underline{\sigma} = \underline{\underline{C}}\left(\underline{\varepsilon} - \underline{\varepsilon}^{th} - \underline{\varepsilon}^{p}\right)$ where $\underline{\underline{C}}$ is the stiffness matrix 6 x 6, $\underline{\sigma}$, $\underline{\varepsilon}$ are, in this case, taken as stress and strain vectors.

$$\dot{\underline{\underline{\varepsilon}}}^{p} = \lambda \frac{\partial f}{\partial \underline{\underline{\sigma}}}$$

$$f = \sqrt{3J_2\left(\underline{\underline{\sigma}} - \underline{\underline{X}}\right)} - \sigma_y$$

$$\dot{\underline{\underline{X}}}_i = c_i\left(\frac{2}{3} a_i \dot{\underline{\underline{\varepsilon}}} - \underline{\underline{X}}_i \dot{p}\right)$$

$$X = \sum_i X_i$$

$$\underline{\underline{C}} = \begin{pmatrix} \lambda + 2G & \lambda & \lambda & 0 & 0 & 0 \\ \lambda & \lambda + 2G & \lambda & 0 & 0 & 0 \\ \lambda & \lambda & \lambda + 2G & 0 & 0 & 0 \\ 0 & 0 & 0 & 2G & 0 & 0 \\ 0 & 0 & 0 & 0 & 2G & 0 \\ 0 & 0 & 0 & 0 & 0 & 2G \end{pmatrix} \quad \text{(eq. 1)}$$

With: $p = \int_0^t \sqrt{\frac{2}{3} \dot{\underline{\underline{\varepsilon}}}^{p} : \dot{\underline{\underline{\varepsilon}}}^{p}}$ $\quad G = \frac{E}{2(1+\nu)}$ $\quad \lambda = \frac{\nu E}{(1+\nu)(1-2\nu)}$ J_2 is the second stress invariant.

Values of coefficients are given in Table 4:

Table 4.
304 L SPLASH and 316 L FAT3D steel parameters identified for non-linear kinematic hardening laws.

Coefficients	E (GPa)	ν	σ_y (MPa)	a_1 (GPa)	a_2 (GPa)	c_1	c_2
304 L SPLASH	175	0.3	102	114	0	532	0
316 L FAT3D	177	0.3	140	114	310	1200	80

4. Fatigue analysis with the French RCC-MR design code

In order to compare thermal fatigue and isothermal fatigue results, a simplified methodology is applied. It is based on the correction of the Poisson effect in the elastic analysis of low cycle fatigue [24], [25]. Such methodology has been used for the French RCC-MR code [19]. Plastic strain can be directly estimated from the strain calculated by assuming a pure elastic behaviour. Thermal fatigue loading on both SPLASH and FAT3D surface virtually corresponds to a perfect biaxial state. It thus undergoes a fictitious equivalent elastic stress range and a corresponding equivalent strain range respectively defined as:

$\Delta\varepsilon_{eq} = K_\nu \Delta\varepsilon_{eq_e}$ Where $\Delta\varepsilon_{eq_e}$ is the elastic strain range as previously deduced and K_ν is a coefficient obtained from the stabilized stress - strain loop.

(eq. 2)

The main steps (eq. 3) are:

1 - Estimation from the cyclic stabilized curve $\Delta\sigma$-$\Delta\varepsilon$ of a secant modulus E_s to take a non-pure elastic behaviour into account.

2 - Estimation of a modified Poisson's value $\bar{\nu}$ (which ranges between 0.3 for elasticity and 0.5 for full plasticity)

3 - Deduction of stress-strain relations deduced from applying the Hooke's elasticity equations.

In that framework, the third relationship corresponds to the perfect biaxial case:

$$E_s = E\frac{\Delta\sigma}{\Delta\sigma_e} \quad (1^{st}) \qquad \bar{\nu} = \nu\frac{E_s}{E} + \frac{1}{2}\left(1 - \frac{E_s}{E}\right) \quad (2^{nd}) \qquad K_\nu = \frac{1+\bar{\nu}}{1+\nu}\frac{1-\nu}{1-\bar{\nu}} \quad (3^{th}) \qquad \text{(eq. 3)}$$

SPLASH: On Fig. 5, test results ($\Delta\varepsilon_{tc}$) obtained for 304 L steel are compared with LCF data obtained with the same heat, at 165 and 320 °C (maximum and medium temperatures of the thermal cycle). In all instances, thermal fatigue results are far lower than uniaxial results. However, such a comparison remains questionable, since the number of cycles required to initiate cracks in Thermal Fatigue conditions are compared to the number of cycles N_{25} to obtain roughly a 3-mm crack length on a cylindrical LCF specimen.

In this framework, LCF curves are modified to estimate the number of cycles required to initiate a 50-µm crack. Such a correction was proposed by [26]:

N_i (50 µm) = $N_R - 12\, N_R^{0.62} + 0.226 N_R^{0.90} + 185$ for $20 \le T \le 600$ °C (eq. 4)

On Fig. 6, the number of cycles required to initiate cracking (as 50-µm to 150-µm crack length) is thus compared under both conditions. It clearly confirms that thermal fatigue is more damaging than uniaxial fatigue.

FAT3D: In Fig. 7, the full curve obtained on 316 L steel at room temperature corresponds to the ($N_R/2$ - $\Delta\varepsilon_t$) endurance curve. Dividing the number of cycles to rupture by a factor of 2 permits the temperature effect to be taken into account, as previously presented on Figure 4, § 2.2.

As for SPLASH tests, Fig. 18 shows that FAT3D results are below LCF results obtained using specimens from the same heat.In all the cases examined, RCC-MR methodology does not give efficient estimations of Thermal Fatigue endurance.

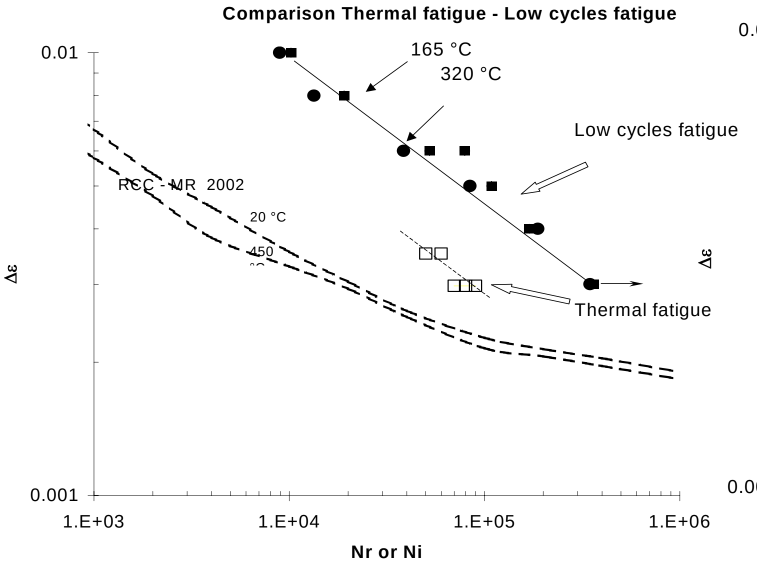

Fig. 5: RCC-MR analysis on SPLASH facility. Comparison between LCF and TF performed on a 304 L steel of the same heat. RCC-MR design curves.

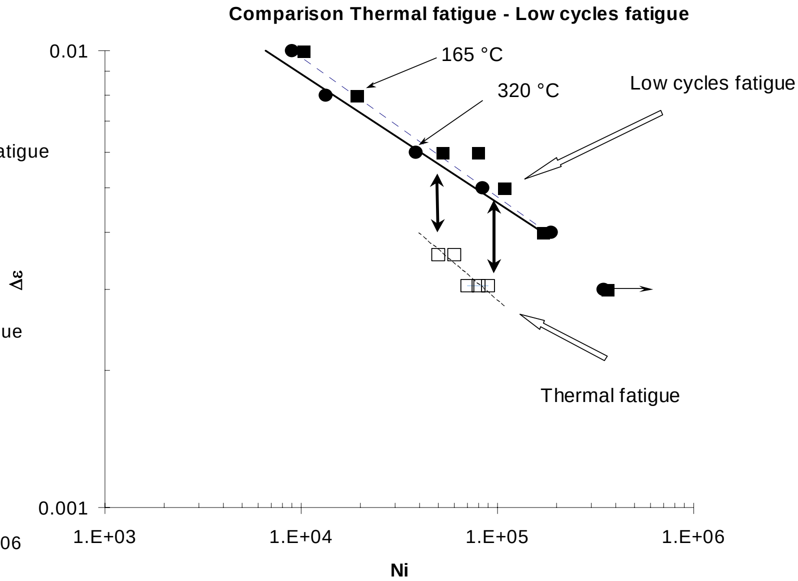

Fig. 6 : RCC-MR analysis on SLASH facility. Number of cycles to crack initiation (50 – 150 μm). Comparison between Thermal Fatigue tests performed on the SPLASH facility and uniaxial fatigue tests.

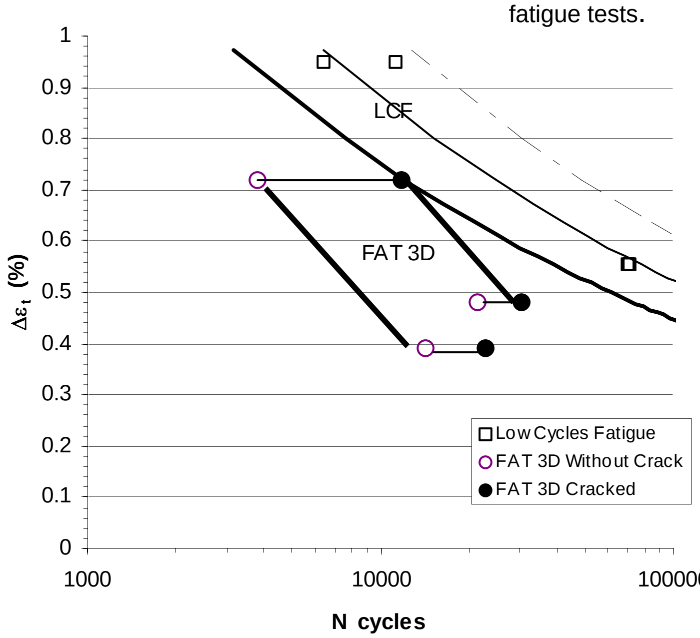

Fig. 7: RCC-MR analysis on FAT3D facility. Comparison between LCF and TF performed on 316 L steel specimens from the same heat.

5. Fatigue analysis using elasto-plastic calculations

Figure 21 summarizes the TF and LCF results. The LCF dotted-line curve represents the number of cycles to rupture (N_{25}). It corresponds approximately to a 3 mm crack. It is built from the ($N_R/2$ - $\Delta\varepsilon_t$) curve obtained on 316 L steel at room temperature and the (N_R - $\Delta\varepsilon_t$) curves obtained on 304 L steel at temperatures of 165 and 320 °C. The LCF full line represents the number of cycles required to initiate a 150-μm long surface crack. It is simply deduced from the LCF dotted-line curve, using eq. 4 [26].

The previously obtained trend is clearly confirmed. Indeed, elasto-plastic calculations do not give efficient estimations on Thermal Fatigue resistance. Thermal fatigue analysis based on equivalent strain (related to the 2nd invariant), is not sufficient.

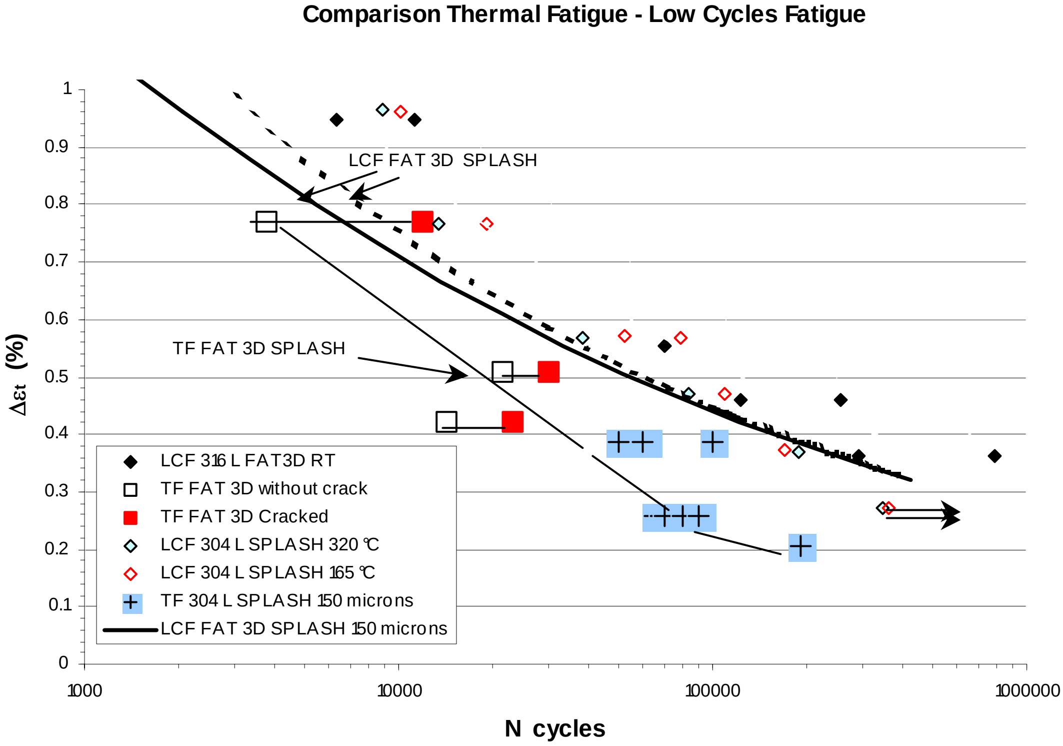

Fig. 8: Complete elasto-plastic calculations on FAT 3D and SPLASH facilities – Comparison with fitted LCF curves.

6. Application of multiaxial fatigue criteria to SPLASH and FAT3D thermal fatigue tests

❖ *Strain criterion proposed by Zamrik* [27]

Equivalent total strain is then given by: $\Delta^{*}\varepsilon_{eq}^{t} = \left(Z^{TF-1}\right)\Delta\varepsilon_{eq}^{e} + \left(\Lambda^{TF-1}\right)\Delta\varepsilon_{eq}^{p}$ (eq. 5)

For type 316 L austenitic stainless steel tested at 621 °C, values are: $Z = 1.42$ and $\Lambda = 2$ [27]. Zamrik's criterion also provides a good estimation for traction and torsion of Haynes 188 material (cobalt base alloy) tested at 760 °C.

Zamrik would seem give best estimations, since SPLASH data are closer than LCF304L data, particularly for the highest number of cycles (Fig. 9).

❖ *Energetic criterion proposed by Ecole Polytechnique-S. Amiable* [28 to 30]:

A new criterion based on energy density has been proposed by [28 to 30]. The stress triaxiality is effectively taking into account, but without introducing the triaxiality factor TF explicitly. The fatigue parameter is simply defined from the dissipated energy and the maximum value of the hydrostatic stress during the stabilized cycle:

$$W^{*} = W_p + \alpha P_{max} \quad \text{(eq. 6)}$$

α is a material parameter without dimension, and: $W_p = \int_{cycle} \sigma : \dot{\varepsilon}^p dt$ $\quad P_{max} = \max_t P(t)$

Let us note that mean stress effect is taken into account since: $W^{*} = W_p + \alpha\left(P_{mean} + P_{amplitude}\right)$

The parameter α can be identified from two tests performed for different triaxiality stress states.

Damage is the sum of two terms:

- the dissipated energy, which is linked to persistent slip band formations, intrusion-extrusions and first micro-cracking.
- a term linked to the hydrostatic pressure, which leads to increasing the crack-opening and developing existent micro-cracking.

The value of α was identified from the thirteen loading paths of traction-torsion [31] as well as the SPLASH thermal fatigue tests. Proposed value was 0.007.

For fully-reversed tension: $W^* = \dfrac{\alpha\sigma_{alt}}{3} + \sigma_{alt}\varepsilon_{p,alt}\dfrac{4(1-n)}{(1+n)}$

Unlimited-endurance limit corresponds to: $W^* = \dfrac{\alpha\sigma_{alt}}{3}$

The criterion proposed by S. Amiable for SPLASH gives the best estimations for the both facilities (Fig. 10). The value of α is also determined from traction-torsion tests [31] including thirteen loading paths. We obtain: $\alpha = 0.007$.

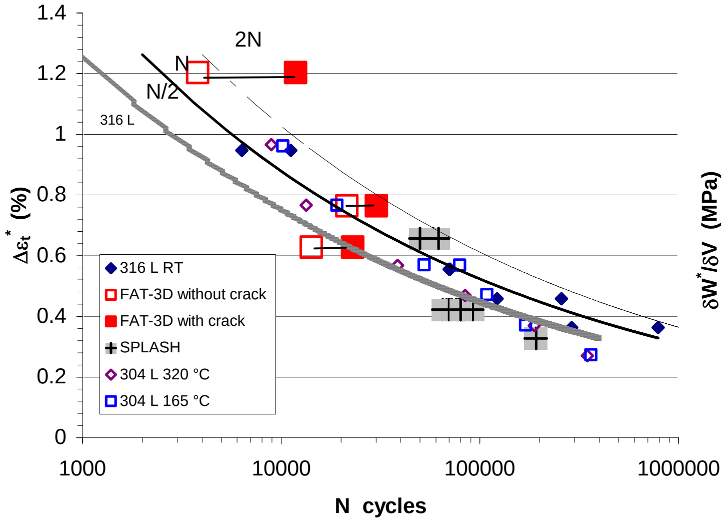

Fig 9: Zamrik's criterion.

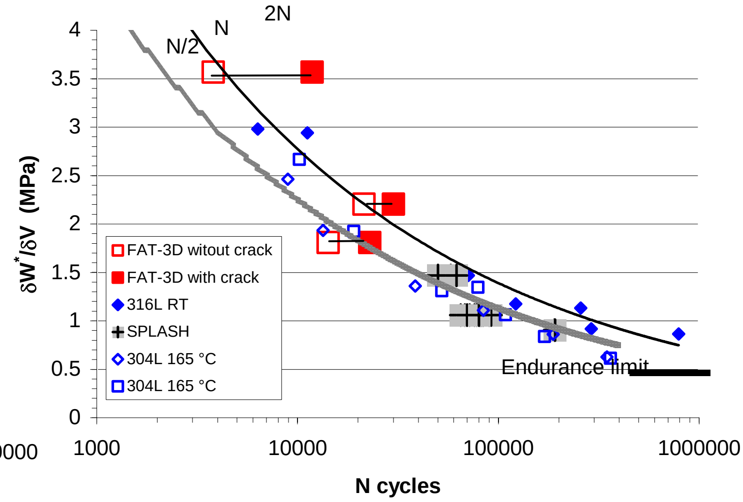

Fig. 10: Criterion proposed in S. Amiable's PhD Thesis (Ecole Polytechnique).

7. Proposition of a suitable multiaxial fatigue criterion.

The objective is to propose a suitable multiaxial fatigue criterion, that is easy to use for design purposes and is also able to give good estimations. In this framework, the two criteria selected are Zamrik's and S. Amiable's.

The first criterion is derived from von Mises equivalent elastic strain $\Delta\varepsilon^{e}_{eq}$ and equivalent plastic strain ranges $\Delta\varepsilon^{p}_{eq}$. In the perfect equibiaxial case, the relation is: $\Delta^*\varepsilon^{t}_{eq} = 1.42\Delta\varepsilon^{e}_{eq} + 2\Delta\varepsilon^{p}_{eq}$ (eq. 6)

In this case, an extension of the RCC-MR method [19] could be considered for applying such a criterion. The value of $\Delta\varepsilon^{t}_{eq}$ could be calculated using the RCC-MR method after an elastic calculation using the K_ν coefficient. Therefore, the value of $\Delta\sigma$ is then simply deduced from:

$$\Delta\varepsilon^{t}_{eq} = \frac{2(1+\nu)}{3}\frac{\Delta\sigma_{eq}}{E} + \left(\frac{\Delta\sigma_{eq}}{K}\right)^n$$

where: E is the Young's modulus, ν is the Poisson's coefficient, K is a plasticity coefficient.

A table giving directly $\Delta\sigma_{eq}$ as a function of $\Delta\varepsilon^{t}_{eq}$ is proposed in the RCC-MR for the Type 316L steel (A3.1S.591). Thereafter, values of $\Delta\varepsilon^{e}_{eq}$ and $\Delta\varepsilon^{p}_{eq}$ are simply deduced.

Regarding Zamrik's criterion applied on SPLASH tests, Fig. 11 compares:
1 - Thermal fatigue estimations as presented in Table I with uniaxial low cycle fatigue data.
2 – The actual method used, where the stress triaxiality is not taken into account, with the proposed method based on Zamrik's criterion.

Let us note that the proposed method provides:

1- A significantly better agreement between LCF and TF results: the very significant discrepancy observed in Fig. 8 disappears.
2- An acceptable agreement between simplified RCC-MR and elastic-plastic calculations.

In that framework, the proposed new method coupling both RCC-MR strain estimations and Zamrik's criterion appears to be more promising for the designer.

8. Conclusion

Some selected criteria have been applied to CEA thermal fatigue tests. As the establishment of a "design criterion" is the objective, only those criteria that are easy to use by an engineer have been selected.

As cyclic plasticity occurs in the endurance domain for austenitic stainless steels, even for a very high number of cycles, criteria based on stress do not seem well adapted. Indeed, criteria based on strain and energy appear to be better adapted. More specifically, the Zamrik's strain criterion proposed by [14 to 15] and the energy criterion proposed by Ecole Polytechnique [28 to 30] provide the best estimations. Let us observe that the application of the Zamrik's criterion using the RCC-MR method is promising, since elastic and plastic parts can be deduced from an elastic calculation and the amplifying factor K_v.

Furthermore, such criteria are well adapted to both SPLASH and FAT3D tests, despite significant differences between experimental processes and approaches developed on both facilities:
- the SPLASH specimen is a "2D specimen", since thermal fatigue results from a in-thickness temperature variation in a free plate. A metallurgical approach is adopted to define crack initiation. It corresponds to the first crack length corresponding to one to two grain sizes on the surface.
- the FAT3D specimen is a "3D specimen", and consequently more representative of in-service components. An approach based on structural mechanics is adopted to define crack initiation. It corresponds to a mechanically significant crack for the structure itself (1 to 2 mm crack length).

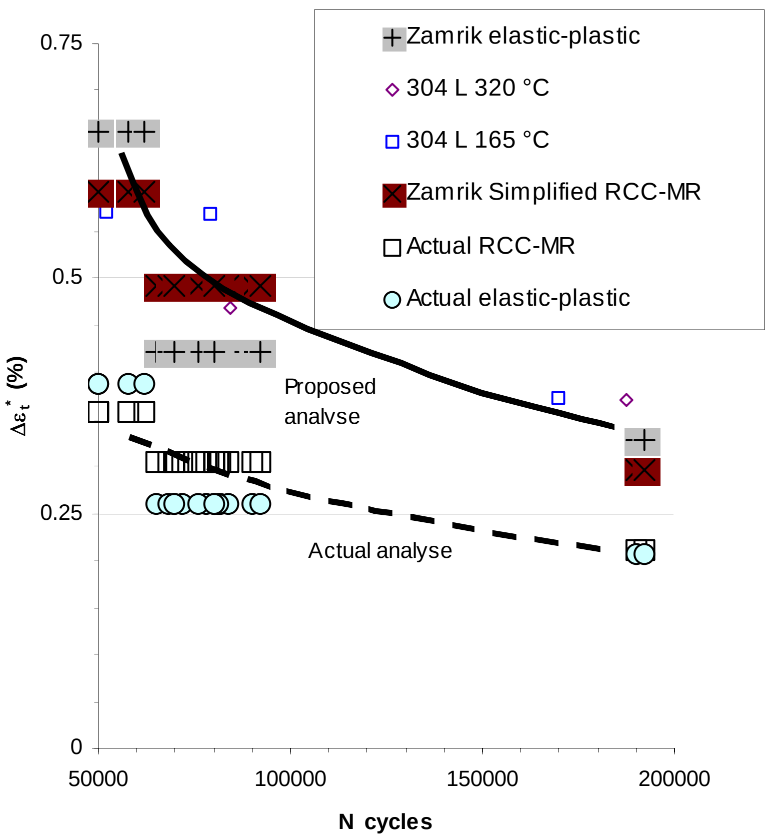

Fig.11: SPLASH tests, comparison between the proposed analysis and the actual analysis, and for the new proposed analysis, comparison between simplified RCC-MR analysis and elastic-plastic calculations.

Acknowledgments:
This work was initiated and supported by the French institute of protection and nuclear safety IRSN

9. References

[1] Spera, D. A., Mowbray, D. F., What is Thermal Fatigue ? Thermal Fatigue of Materials and Components. ASTM STP 612, 1976, pp. 3 - 9.
[2] Bressers, J., Rémy, L. Fatigue under Thermal and Mechanical Loading. Kluwer, 1996.
[3] Burlet, H., Vasseur, S., Cailletaud, G., Pineau, A. Fatigue Crack Growth Under thermomechanical Loading – Application to Life Prediction of Centrifugal Casting Equipment. High Temp Fract Mechanisms and Mechanics EGF 6, Mechanical Eng Pub, 1990, pp. 379–395.
[4] De Keroulas, F. , B. Thomeret, B. , In French, Fissuration par fatigue thermique de tuyauteries auxiliaires du circuit primaire principal : analyse des cas rencontrés – Contribution des expertises sur matériaux à la résolution des problèmes rencontrés dans les réacteurs à eau pressurisée, SFEN, 1990. Vol. 1 312, pp. 107 – 117.
[5] Crutzen, S., Birac, C., Champigny, F., Dugue, C., Benoist, P. Programme for inspection of steel components, Int Symp Fontevraud 3, 1994, Vol. 1.
[6] Cipière M. F., Le Duff J. A.. Thermal fatigue experience in French piping Int. Inst. Of Welding, 2001, Document n° XIII – 1891 – 01, Lubjana, Slovenia.
[7] Stephan, J. M., Curtit, F., Vinndeirinho, C., Taheri, S., Akamatsu, M., Peniguel, C., 2002. Evaluation of the risk of damages in mixing zones, Fatigue 2002, Blom, A. F. Editors, EMAS 3 pp. 1707 – 1714.
[8] Fissolo, A., Forestier, A., Chapuliot, S., Gourdin, C., Magnaud, J. P., Ducros, F., Quéméré, P., Emonot, P., Chatelain, A., Dolias, Y., Braillard, O., Vincent, L., Robertson, C., Guilbaud, D., Le Corre, V., Maillot, V., Haddar, N., Amiable, S., Constantinescu, A., Degallaix, G., Degallaix, S. Advances in Thermal Fatigue investigations performed in CEA for French PWR piping, Proceedings of Third Int Conf on Fatigue of Reac Comp, EPRI, US NRC, OECD NEA, 2004, Sevilla, Spain.
[9] Fissolo, A., Marini, B., Nais, G., Wident, P. Thermal fatigue behaviour for a 316L type steel. J of Nucl Mater (Netherlands) 1996; 233-237 (1-3): 156–161.
[10] Maillot, V. Amorçage et propagation de réseaux de fissures de fatigue thermique dans un acier inoxydable austenitique de type X2 CrNi18-09 (AISI 304L), CEA report R-6041, 2003, PhD Thesis, Ecole Centrale de Lille.
[11] Maillot, V., Degallaix, G., Degallaix, S., Fissolo, A., 2006. Biaxial thermomechanical fatigue on 304 L-type austenitic stainless steel, MP Materialprüfung 2006; 48(1–2): 43 – 49.
[12] Fissolo, A. Fissuration en fatigue thermique des aciers inoxydables austénitiques, CEA Report R-5982, Mémoire d'Habilitation à Diriger les Recherches 2001, Université des Sciences et Technologie de Lille.
[13] Chapuliot, S., Ancelet, O., Payen, T., Mathet, E. OCDE Benchmark on thermal fatigue problem, Proceedings of the Third Conf on Fatigue of React Comp, EPRI, US NRC, OECD NEA, 2004, Sevilla, Spain.
[14] Ancelet, O. Etude de l'amorçage et de la propagation des fissures sous chargement cyclique, CEA Report R-6109, PhD Thesis, 2006, University of Poitiers, France.
[15] Ancelet, O., Chapuliot, S. , Hennaf, G. , Marie, S. Development of a test for the analysis of the harmfulness of a 3D thermal fatigue loadings in tubes. Int J of Fatigue 2007; 29: 549 –564.
[16] Vincent L., Malésys N., Chaise S. , Perez G., Fatigue à grand nombre de cycles d'un acier inoxydable austénitique, Colloque National MECAMAT 2007, Aussois, France.
[17] Maillot, V., Degallaix, G., Degallaix, S., Fissolo. A. Thermal fatigue crack networks parameters and stability: an experimental study. Int J of Solids and Structures, Special issue: Micromechanics of Materials - Edited by Mark Kachanov; 2004, 42/2: 759-769.
[18] Petrequin, P., Mottot, M., Rabbe, P., Amzallag, C., Vallibus, L., Grattier, G. Allowing for Low Cycle Fatigue in the construction of Fast Sodium Cooled Reactors, Mécanique Matériaux, Eléctricité; 323/324: 34-41.
[19] RCC-MR French code, Association Française pour les Règles de conception et de construction des Chaudières Electro-Nucléaires, Edition 2002.
[20] Constantinescu, A., Charkaluk, E., Lederer, G., Verger, L. A computional approach to thermomechanical fatigue. Int J of Fatigue 2004; 26: 805-818.
[21] Thomas, J.J., Verger, L., Bignonnet, A., Charkaluk, E. Thermomechanical design in the automotive industry. Fat and Fract of Eng Mater and Struct, 2004; 27 (10): 887-895.
[22] Gerland,M., Alain, R., Ait Saadi, B. , Mendez, J. Low cycle fatigue behaviour in vacuum of a 316L-type austenitic stainless steel between 20 and 600 °C. II Dislocation structure evolution and correlation with cyclic behavior, Mat. Science and Engineering A 1997; A229 (1-2): 68-86.
[23] Lemaitre, J., Chaboche, J.L. Mécanique des matériaux solides. Dunod, 1998.
[24] Roche, R. L. Correction for Poisson's effect in the elastic analysis of low cycle fatigue, 1984, Note CEA - N 2389.
[25] Moulin D., Roche R. L. Int J of Pressure Ves and Piping, 1985; 19: 213-233.
[26] Levaillant C. Approche métallographique de l'endommagement d'aciers inoxydables austénitiques sollicités en fatigue plastique ou en fluage, PhD Thesis 1984, University of Technology of Compiègne.
[27] Zamrik, S. Y., Mirdamadi, M. Davis, D. C. A proposed model for biaxial fatigue analysis using the triaxiality factor concept. Advances in Multiaxial Fatigue. ASTM STP 1191, Mc Dowell/ Ellis Editor, 1993, pp. 85-106.
[28] Amiable, S. , Chapuliot, S ., Constantinescu, A., Fissolo, A. Prédiction de durée de vie sous chargement de fatigue thermique. 17ème Congrès Français de Mécanique, 2005, Troyes, France.
[29] Amiable, S. , Chapuliot, S ., Constantinescu, A., Fissolo, A.. 2005. A comparison of lifetime prediction methods for a thermal fatigue experiment. Int J of Fatigue 2006; 28(7):692-706.
[30] Amiable , S. Prédiction de durée de vie des structures sous chargement de fatigue thermique. PhD Thesis, 2006, Université de Versailles.
[31] Itoh, T., Sakane, M., Ohnami, M., and Socie, D. Nonproportional low cycle fatigue criterion for type 304 stainless steel. J of Eng Mater and Tech (Transactions of the ASME) 1995, 117(3) :285-292.